

# Power Spectra in Global Defect theories of Cosmic Structure Formation

Ue-Li Pen <sup>\*</sup>, Uroš Seljak <sup>†</sup>, and Neil Turok<sup>‡</sup>

<sup>\*</sup> *Harvard College Observatory, 60 Garden St., Cambridge MA 02138*

<sup>†</sup> *Harvard-Smithsonian Center for Astrophysics, 60 Garden St., Cambridge MA 02138*

<sup>‡</sup> *DAMTP, Silver St, Cambridge, CB3 9EW, U.K.*

(September 6, 2018)

An efficient technique for computing perturbation power spectra in field ordering theories of cosmic structure formation is introduced, enabling computations to be carried out with unprecedented precision. Large scale simulations are used to measure unequal time correlators of the source stress energy, taking advantage of scaling during matter and radiation domination, and causality, to make optimal use of the available dynamic range. The correlators are then re-expressed in terms of a sum of eigenvector products, a representation which we argue is optimal, enabling the computation of the final power spectra to be performed at high accuracy. Microwave anisotropy and matter perturbation power spectra for global strings, monopoles, textures and non-topological textures are presented and compared with recent observations.

## I. INTRODUCTION

Over the next few years high resolution maps of the cosmic microwave sky will become available. These maps will allow competing theories of cosmic structure formation to be tested with exquisite precision. The primary quantities of interest for comparing theories to observations are the power spectra of fluctuations, both for the microwave sky temperature and the mass density. The predictions of simple inflationary theories have largely been worked out, typically to one per cent accuracy, and detailed comparisons with data are taking place. The state of the main rival set of theories, based on symmetry breaking and phase ordering, has been less rosy. These theories involve a causal source comprising the ordering fields and/or defects, which continually perturbs the universe on ever larger scales. In the inflationary theories, linear perturbation evolution is all that is needed: but for the defect theories full linear response theory is required. The defect sources are in general ‘decoherent’ [1], providing additional computational difficulty. This Letter presents a general solution method for solving the linear response problem in such models.

## II. STIFF SOURCES: MEASURING UNEQUAL TIME CORRELATORS

Accurate codes have been developed for field evolution in different symmetry breaking theories. But a single simulation cannot simultaneously resolve all scales of observational relevance. Thus information gathered from simulations must be combined in some way. It has been clear for some time that the ideal quantity which a) uses all the information present in a simulation, b) incorporates the powerful properties of scaling evolution and causality, and c) preserves all the information needed to compute power spectra is the unequal time correlator (UETC) of the defect source stress energy tensor  $\Theta_{\mu\nu}$ :

$$\langle \Theta_{\mu\nu}(\mathbf{k}, \tau) \Theta_{\rho\lambda}(-\mathbf{k}, \tau') \rangle \equiv \mathcal{C}_{\mu\nu, \rho\lambda}(k, \tau, \tau') \quad (1)$$

where  $\tau, \tau'$  denote conformal time, and  $k$  comoving wavenumber. Because the perturbed Einstein-matter equations are linear, all perturbations are determined in terms of the source via appropriate Greens functions. Thus in principle all quadratic estimators of the density perturbations are determined by (1).

The unequal time correlators are highly constrained by causality, scaling and stress energy conservation. Causality means that the real space correlators of the fluctuating part of  $\Theta_{\mu\nu}$  must be zero for  $r > \tau + \tau'$  [2]. Scaling [3] dictates that in the pure matter or radiation eras  $\mathcal{C}_{\mu\nu, \rho\lambda} \propto \phi_0^4 / (\tau \tau')^{\frac{1}{2}} c_{\mu\nu, \rho\lambda}(k\tau, k\tau')$ , where  $\phi_0$  is the symmetry breaking scale and  $c$  is a scaling function. Finally, energy and momentum conservation for the stiff source (see e.g. [3]) provide two linear constraints on the four scalar components of the source. Any pair determines the other two up to possible integration constants. In our work we have found the best pair to be the energy density  $\Theta_{00}$  and the anisotropic stress  $\Theta^S$ ; the energy and momentum conservation equations give good behavior for all components on both superhorizon and subhorizon scales. This choice is also favoured by the fact that  $\Theta_{00}$  and  $\Theta^S$ , along with the vector and tensor components,  $\Theta^V$  and  $\Theta^T$  fix all superhorizon perturbations in the most direct manner. However, we have also checked that other choices give consistent results.

As mentioned, our method uses scaling and causality to extend the dynamic range of the numerical simulations. In the simulations, the fields start from uncorrelated, but non-scaling initial conditions, and evolve towards scaling behaviour. We evolve the fields to some final time  $\tau$  when the system is well into the scaling regime. At this time we compute the stress energy tensor  $\Theta_{\mu\nu}$ , which we Fast Fourier Transform and decompose into the variables  $\Theta_{00}$ ,  $\Theta^S$ ,  $\Theta^V$ , and  $\Theta^T$ . We then repeat the simulation with identical initial conditions, computing the same quantities at several times  $\tau' \leq \tau$ . This procedure

ensures that the equal time correlations, which dominate the perturbation production, are measured when the system is closest to scaling. We store the isotropic averages of the correlators as functions of the wave vector magnitude  $k$ , e.g.  $\mathcal{C}_{00,S}(k\tau, \tau'/\tau) = \langle \Theta_{00}(\mathbf{k}, \tau) \Theta^S(-\mathbf{k}, \tau') \rangle$ . Statistical and sampling errors are small at large  $k$  because many modes contribute, but at small  $k$  the sampling is sparse and the noise larger. In particular the value at  $k = 0$  represents the mean defect density and should be discarded. In order to increase the resolution for small  $k\tau$ , we compute the correlators in real space and project them onto the radial separation  $r$ . The fact that the correlators must vanish for  $r > \tau + \tau'$  allows us to solve for an additive constant, in effect determining the  $k = 0$  value. The projected real space correlator is then transformed back to Fourier space using the continuum Fourier transform over the compact support  $\mathcal{C}(k) = 4\pi \int_0^{\tau+\tau'} r^2 dr \mathcal{C}(r) \sin(kr)/kr$ . For small values of  $k$  we use the latter equation, while for large values we use the direct Fourier space computation. For intermediate  $k\tau \sim 5$  the two match well, but this procedure allows us to extend our dynamic range in small  $k\tau$  by an order of magnitude. Note that using causality in this way limits the final time in the simulation to  $\tau < \frac{L}{4}$  where  $L$  is the box size; typically we evolve in a  $400^3$  box to  $\tau = \frac{L}{8} = 50$  so that there are still many independent horizon volumes in the box.

### III. EIGENVECTOR PRODUCT REPRESENTATION

We have explained how one can devote the full numerical power at hand to compute the UETCs alone, without wasting computational effort or storage on linear perturbation theory. Next we shall show how very fast Einstein-Boltzmann solvers recently developed [5] can be used to convert the UETCs into cosmological power spectra with relatively small numerical effort and very high precision.

This is done by representing the UETCs as a sum of eigenvector products [2]. The idea is to regard the stress energy correlators (1) as ‘symmetric matrices’ with indices  $\mu\nu, \tau$  and  $\rho\lambda\tau'$ . In practise, to compute the scalar perturbations we need the auto- and cross-correlators of two components (for example  $\Theta_{00}$  and  $\Theta^S$ ), and for the vector and tensor perturbations we need the two auto-correlators of  $\Theta^V$  and  $\Theta^T$ . Regarded as matrices, the correlators involved are symmetric and positive definite (expectation values of squares) and so the eigenvalues are all real and positive. Matrix index summation is replaced with an integral  $\int d\tau w(\tau)$  with  $w(\tau)$  some chosen weighting function. Often the choice of weighting is naturally dictated by scaling and dimensional analysis, but in any case the results were checked to be independent of it. For sensible choices of  $w(\tau)$  the trace of the corre-

lators is finite: it follows that there is a convergent series of positive eigenvalues which may be used to index the eigenvector sum. The correlators can then be expressed as an infinite sum

$$\mathcal{C}(k, \tau, \tau') = \sum_i \lambda^i v^i(k, \tau) v^i(k, \tau'), \quad (2)$$

where

$$\int d\tau' \mathcal{C}(k, \tau, \tau') v^i(k, \tau') w(\tau') = \lambda^i v^i(k, \tau). \quad (3)$$

The indices labelling the components of the stress tensor are implicit. We have found that including the largest 15 eigenvectors typically reproduces the unequal time correlators to better than ten per cent precision: the effect of including more than 15 on the final perturbation power spectra is negligible at the few per cent level.

We believe the properties of this representation make it ideal for the purpose of computing cosmological perturbations. Namely a) the representation automatically minimises the ‘least squares’ fit, for a given number of eigenvectors b) the eigenvectors individually conserve stress energy c) the eigenvectors individually vanish as  $\tau$  goes to zero since the correlators  $\mathcal{C}(k, \tau, \tau')$  vanish for  $\tau \ll \tau'$ , making specification of the initial conditions trivial, and d) the contribution of successive eigenvectors to the perturbations converges quickly, as a result both of the decrease in eigenvalue and the increasingly oscillatory nature of the eigenvectors. In particular the incoherent superhorizon ( $k\tau < 1$ ) portion of the correlators is represented by an infinite sum of ever more oscillatory eigenfunctions, which have increasingly little effect on the perturbations. For the computation we discretise the unequal time correlators sampled in 256 equal logarithmic spacings in the interval  $e^{-6.4} \leq k\tau \leq e^{9.6}$ . The individual eigenvectors are each fed into a full Boltzmann code [5], and the total perturbation power spectra are then given by the sum of those for individual eigenvectors, weighted by their eigenvalue.

During the pure matter and radiation epochs, the procedure is simplified because the correlators scale, and so are represented for all  $k$  by a single set of eigenvectors, functions of  $k\tau$ . We incorporate the matter-radiation transition by repeating the computation of unequal time correlators for several different values (typically 20) of  $\tau/\tau^*$ , where  $\tau^*$  is the conformal time at matter-radiation equality  $\Omega_r(\tau^*) = \Omega_m(\tau^*)$ . After the simulations are completed, we collect the results in a matrix of correlators,  $\mathbf{\Xi}(k\tau, k\tau', k\tau^*)$ , which are then diagonalised to produce a set of eigenvectors for each  $k\tau^*$  considered. These eigenvectors smoothly interpolate between those for the radiation era and those for the matter era, so the Boltzmann code can use a simple spline interpolation between them. The integration solves the full linearised relativistic Einstein equations tracking the

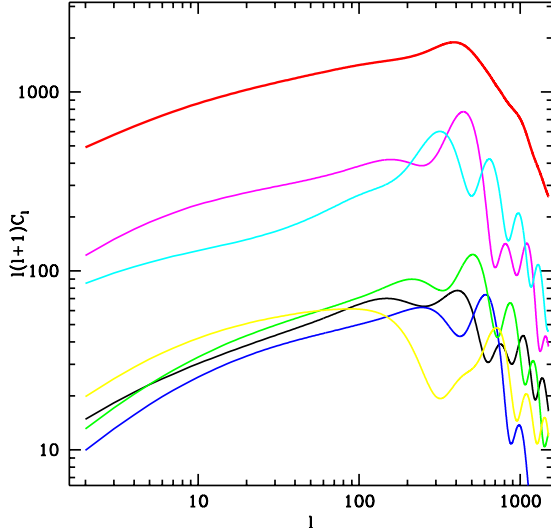


FIG. 1. Angular power spectrum of anisotropies generated by the scalar component of the source stress energy for global strings. The upper curve shows the total spectrum, the lower ones contributions from individual eigenvectors. This Figure illustrates decoherence: each eigenvector individually produces an oscillatory  $C_l$  spectrum, but these oscillations all cancel in the sum.

photons  $\delta_r$ , baryons  $\delta_b$ , cold dark matter  $\delta_c$ , neutrinos  $\delta_\nu$ , and their relative couplings. The evolution includes the full matter-radiation transition, finite recombination rate, and other effects. The Boltzmann calculations are accurate to about 1%.

#### IV. CHECKS

Many checks have been performed on this procedure, which we briefly summarise here [4]. When the box size of texture simulations is reduced from  $400^3$  to  $256^3$ , the  $C_l$  spectrum changes by less than 3%. To check consistency with energy conservation we used a different pair of scalar variables  $\Theta_{00} + \Theta$ ,  $\Theta + 2\Theta^S$ , which changed the results by 5%, in  $400^3$  boxes, but the latter pair gave much slower convergence with box size. Weighting the diagonalisation by an additional factor of  $\tau^{1/2}$  adds more weight to subhorizon scales, and affects the result by up to 10% at  $l = 2$ , but less than 2% at larger  $l$ . We have compared the total, as well as scalar, vector and tensor anisotropies to those produced by the direct line-of-sight integration code [3], and they individually agree to 10-20%. Since the current method includes additional contributions at the last scattering surface, explicitly uses scaling, employs far larger box sizes, and more accurate integrations, we conclude the results are consistent with the new results being much more accurate. All these checks indicate that these new results are reliable to better than 10% [7].

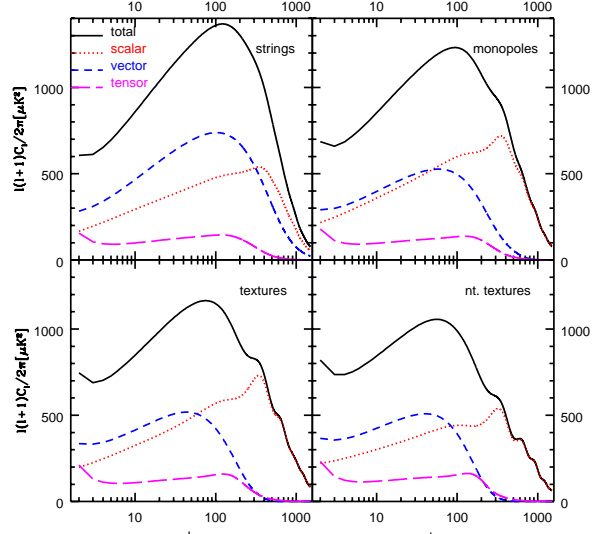


FIG. 2. The contributions to the total power from scalar, vector and tensor components.

#### V. RESULTS

The resulting angular power spectrum of the temperature anisotropies for the scalar perturbations sourced by global cosmic strings are shown in Figure 1. Each of the eigenmodes is coherent and shows the expected acoustic peaks [6]. Decoherence is manifested when we sum over eigenvectors. The peaks add out of phase, resulting in a smooth angular power spectrum. One expects cosmic strings to be the least coherent of the defects under consideration. Indeed, the  $N = 6$  non-topological texture scalar modes do exhibit residual oscillations even when summed over all eigenmodes as shown in Figure 2. The figures show  $C_l$  spectra computed for  $h = 0.5, \Omega_b = 0.05, \Omega = 1$ . The dependence on the Hubble constant  $h$  and baryon content  $\Omega_b$  is weak [4]. The most striking feature of all the models under consideration is the predominance of vector modes. They dominate up to  $l \sim 100$ , at which point they are suppressed by the horizon size on the surface of last scatter. It is not hard to see that vector and tensor contributions should be at least comparable to the scalar contribution. By causality the  $k$  space correlator is an integral over a real space function of compact support, and should be analytic in  $k$  at small  $k$ . By isotropy, we can expand any correlator at small  $k\tau$  as  $c_{ij,kl}(k\tau, k\tau') = A\delta_{ij}\delta_{kl} + B(\delta_{ik}\delta_{jl} + \delta_{il}\delta_{jk}) + O(k^2)$ . The constant  $A$  contributes only to trace correlators: the single constant  $B$  then determines the anisotropic scalar, vector and tensor contributions, in the ratios  $c_{S,S} : c_{V,V} : c_{T,T} = 3 : 2 : 4$  (these are accurately verified in our simulations). Thus vectors and tensors can be expected to contribute a significant fraction of the temperature anisotropies in field ordering theories. (A general analysis of the relative im-

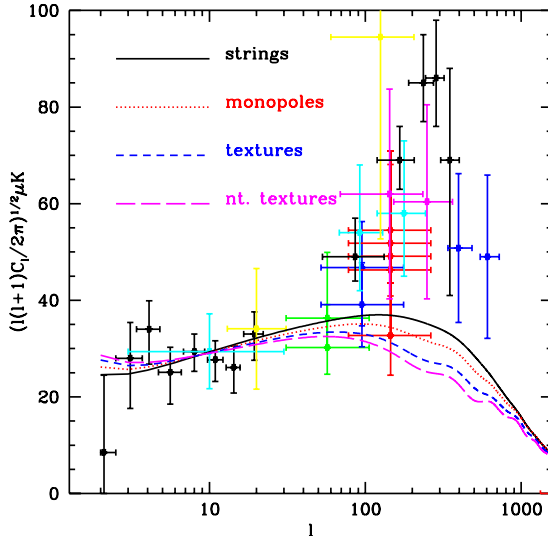


FIG. 3. Comparison of defect model predictions to current experimental data. All models were COBE normalised at  $l = 10$ .

portance of vector and tensor modes will be described elsewhere [4].) The large amplitude of vector modes and the decoherent sum of eigenmodes leads to a suppression of power at  $l \gtrsim 100$  [8], a very different spectrum to that expected from adiabatic fluctuations in inflationary models. We show a comparison between the predictions of the global field defect theories and the current generation of CMB experiments in Figure 3. All models are normalised to COBE at  $l = 10$ . They are all systematically lower than the current degree-scale experimental points.

The same calculations directly yield the matter power spectrum shown in Figure 4. Normalised to COBE, our tests indicate that the results should be reliable to a few percent. From the power spectra we derive the normalization  $\sigma_8$  of the matter fluctuation in  $8h^{-1}$  Mpc spheres. Global strings, monopoles, texture and  $N = 6$  non-topological texture give  $\sigma_8 = 0.26, 0.25, 0.23, 0.21$ , respectively, for  $h = 0.5$ , and scaling approximately as  $h$ . The field normalization for textures is  $\epsilon = 8\pi^2 G\phi_0^2 = 1.0 \times 10^{-4}$ , consistent with our previous calculation [3] of  $\epsilon = 1.1 \times 10^{-4}$ . These normalizations are a factor of 5 lower than the generic prediction of  $n = 1$  inflationary models where  $\sigma_8 = 1.2$  for  $h = 0.5$ . Cluster abundances suggest values of  $\sigma_8 \sim 0.5$  for a flat universe.

To summarise, the techniques used here enable us to convert unequal time correlators into temperature anisotropy and matter fluctuation power spectra within a few hours on a workstation. For all the defect theories, vectors contribute approximately half of the total CMB anisotropy on large scales, leading to a suppression of acoustic peaks and a low normalization of the matter power spectrum  $\sigma_8 \sim 0.25h_{50}$ . Current observations of

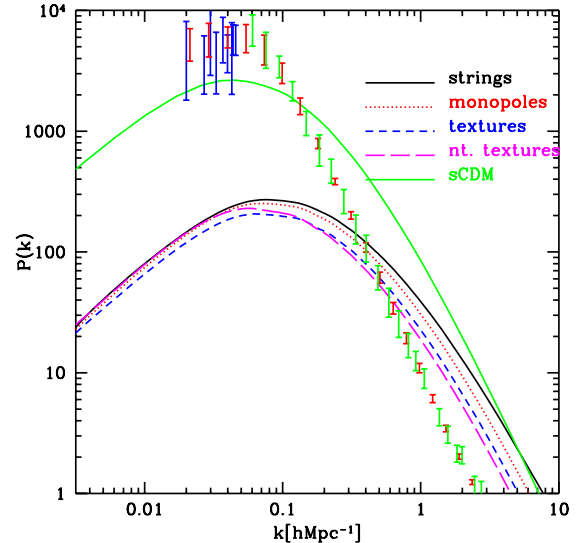


FIG. 4. Matter power spectra computed from the Boltzmann code summed over the eigenmodes. The upper curve shows the standard cold dark matter (sCDM) power spectrum. The defects generally have more power on small scales than large scales relative to the adiabatic sCDM model. The data points show the mass power spectrum as inferred from the galaxy distribution [9].

CMB anisotropies and galaxy clustering do not favor the models under consideration.

We thank Robert Crittenden, Robert Caldwell and Lloyd Knox for helpful discussions and John Peacock and Max Tegmark for providing observational data points. This research was conducted in cooperation with Silicon Graphics/Cray Research utilising the Origin 2000 supercomputer as part of the UK-CCC facility supported by HEFCE and PPARC (UK).

---

- [1] A. Albrecht, D. Coulson, P. Ferreira and J. Magueijo, Phys. Rev. Lett. **76**, 1413 (1996).
- [2] N. Turok, Phys. Rev. **D54**, 3686 (1996), Phys. Rev. Lett., **77**, 4138 (1996).
- [3] U. Pen, D. Spergel and N. Turok, Phys. Rev. **D48**, 692 (1994).
- [4] U. Pen, U. Seljak and N. Turok, 1997, in preparation.
- [5] U. Seljak and M. Zaldarriaga, Astrophys. J. **469**, 437 (1996).
- [6] R. Crittenden and N. Turok, Phys. Rev. Lett. **75**, 2642 (1995).
- [7] Differences between our results and those of [6] are due to a) larger vector and tensor amplitudes (a factor of 3) and b) the effects of source incoherence reducing the scalar ‘Doppler’ peak by a factor of 2.
- [8] We are aware of computations in progress for local strings by B. Allen *et al.* which indicate qualitatively similar results.
- [9] J.A. Peacock, M.N.R.A.S. **284**, 885 (1997).

